Chin. Geogra. Sci. 2019 Vol. 29 No. 4 pp. 679–688
https://doi.org/10.1007/s11769-019-1052-0

Springer Science Press
www.springerlink.com/content/1002-0063

Spatio-temporal Characteristics of Area Coverage and Observation Geometry of the MISR Land-surface BRF Product: A Case Study of the Central Part of Northeast Asia

LI Jian[1], CHEN Shengbo[1], QIN Wenhan[1], Mike MUREFU[1], WANG Yufei[2], YU Yan[1], ZHEN Zhijun[1]

(1. *College of Geo-Exploration Science and Technology*, *Jilin University*, *Changchun* 130026, *China*; 2. *Climate Centre of Jilin Province*, *Changchun* 130062, *China*)

Abstract: The Multi-angle imaging spectroradiometer (MISR) land-surface (LS) bidirectional reflectance factor (BRF) product (MILS_BRF) has unique semi-simultaneous multi-angle sampling and global coverage. However, unlike on-satellite observations, the spatio-temporal characteristics of MILS_BRF data have rarely been explicitly and comprehensively analysed. Results from 5-yr (2011–2015) of MILS_BRF dataset from a typical region in central Northeast Asia as the study area showed that the monthly area coverage as well as MILS_BRF data quantity varies significantly, from the highest in October (99.05%) through median in June/July (78.09%/75.21%) to lowest in January (18.97%), and a large data-vacant area exists in the study area during four consecutive winter months (December through March). The data-vacant area is mainly composed of crop lands and cropland/natural vegetation mosaic. The amount of data within the principal plane (PP) ±30° (nPP) or cross PP ±30° (nCP), varies intra-annually with significant differences from different view zeniths or forward/backward scattering directions. For example, multiple off-nadir cameras have nPP but no nCP data for up to six months (September through February), with the opposite occurring in June and July. This study provides explicit and comprehensive information about the spatio-temporal characteristics of product coverage and observation geometry of MILS_BRF in the study area. Results provide required user reference information for MILS_BRF to evaluate performance of BRDF models or to compare with other satellite-derived BRF or albedo products. Comparing this final product to on-satellite observations, what was found here reveals a new perspective on product spatial coverage and observation geometry for multi-angle remote sensing.

Keywords: multi-angle remote sensing; Multi-angle Imaging Spectroradiometer (MISR); bidirectional reflectance factor (BRF); spatio-temporal characteristics; observation geometry

Citation: LI Jian, CHEN Shengbo, QIN Wenhan, Mike MUREFU, WANG Yufei, YU Yan, ZHEN Zhijun, 2019. Spatio-temporal Characteristics of Area Coverage and Observation Geometry of the MISR Land-surface BRF Product: A Case Study of the Central Part of Northeast Asia. *Chinese Geographical Science*, 29(4): 679–688. https://doi.org/10.1007/s11769-019-1052-0

1 Introduction

The Multi-angle Imaging SpectroRadiometer (MISR) onboard the Terra satellite semi-simultaneously observes land surface and atmospheric systems at nine angles. The MISR land-surface (LS) bidirectional reflectance factor (BRF) product (MILS_BRF), often acts as the reference dataset for various bi-directional reflectance distribution function (BRDF) models (Chen et al., 2008; Wu et al., 2011; Czapla-Myers et al., 2014). As such, it is one of the most important data sources for the calculation of global dynamic land-surface BRDFs (Wanner et al., 1997). However, due to the influence of atmospheric conditions, diversity of land surface covers, com-

Received date: 2018-09-10; accepted date: 2019-01-04
Foundation item: Under the auspices the Fundamental Research Funds for the Central Universities, China (No. 2017TD-26), the Plan for Changbai Mountain Scholars of Jilin Province, China (No. JJLZ[2015]54)
Corresponding author: CHEN Shengbo. E-mail: chensb@jlu.edu.cn
© Science Press, Northeast Institute of Geography and Agroecology, CAS and Springer-Verlag GmbH Germany, part of Springer Nature 2019

plicated terrain conditions and performance of inversion models, among other factors, the MISR on-satellite observations can not all be converted to land-surface BRF data (Diner et al., 2008). Therefore, the spatio-temporal characteristics of on-satellite observations and of MILS_BRF are not equivalent. Many studies and applications have used analysis of spatio-temporal characteristics of area coverage and observation geometry of MILS_BRF, including: 1) BRDF model evaluation (Chen et al., 2008) or error source analysis based on MILS_BRF (Lucht, 1998; Lucht and Lewis, 2000); 2) selection of high quality data when using MISR data for land surface classification (Armston et al., 2007; Liu and Kafatos, 2007; Mahtab et al., 2008); 3) evaluation of sensor calibration accuracy (Bruegge et al., 2014; Angal et al., 2017) or the accuracy of the albedo based on long time data series (Taberner et al., 2010; Pinty et al., 2011; He et al., 2017); 4) analysis of expanding MISR multi-angle remote sensing capability through multiple small satellites (Nag et al., 2015, 2017). However, the area coverage and observation geometry characteristics of MILS_BRF in these studies are often ignored or lack explicit analysis and detailed consideration of the product's spatio-temporal features.

When used in a specific region, a number of questions regarding MILS_BRF remain unanswered. What is the overall coverage rate of the product? Is the amount of available data similar among months, locations, or land covers? If significant differences exist, how are they distributed? What are the characteristics of observation geometry in entire year and how does it change by month? These questions have not been explicitly answered but are important to the research or applications using MILS_BRF.

The objective of this study is to analyze and obtain comprehensive and explicit information about the spatio-temporal distribution characteristics of MILS_BRF and its observation limitations. The information will provide a reference guide for the work of BRDF models and/or product accuracy evaluation using MILS_BRF as benchmark data. To achieve this goal, we study a typical region in central Northeast Asia, using the MILS_BRF over a 5-yr period as an example. We analyzed the spatio-temporal characteristics of the product coverage as well as the overall annual and intra-annual characteristics of its observation geometry.

2 Materials and Methods

2.1 Study area

The study area is located in the central part of Northeast Asia covering approximately 67 000 km^2 (Fig.1(a)). It is characterized by a temperate continental monsoon climate. The precipitation in the area is concentrated during June to August. During winter, most parts of the area have heaped snow covers. Land use and cover types in the study area cover most major types found in the International Geosphere-Biosphere Programme (IGBP) classification system (LP DAAC, 2017) for the greater region (Fig. 1(b)). The north-western part of the study area, with relatively flat terrain, is an agricultural area greatly affected by human activities while the central and eastern parts are dominated by forest-covered mountains. Residential communities of various sizes are scattered across the study area. Vegetation in the area has notable phenological variation with a growing season from April to October and a dormant season from November to March.

2.2 Data and methods

The MILS_BRF datasets (Bull et al., 2011; MISR-Science-Team, 2015a) from 2011 through 2015 in the study area were assembled. Imaging dates on which the product coverage rate of the study area is greater than 10% were selected (Table 1). From this set the view-sun relative azimuths and view zenith angles corresponding to BRF data of each pixel in the study area were extracted. Based on the 5-yr cumulative data, monthly characteristics of the product coverage rate and location together with the whole-year overall characteristics of the view-target-sun geometry and its intra-annual variation were statistically analyzed.

For all MILS_BRF data, view zeniths and view-sun relative azimuths were divided into nine and three groups, respectively. As result, a total of 27 kinds of observation geometries were considered. View zenith angles were grouped by MISR cameras. Observations from forward looking cameras (Df, Cf, Bf and Af) represent the energy of forward-scattered sunlight from the land surface in the nominal view zenith angles of 70.50°, 60.0°, 45.6° and 26.1° respectively. Conversely, observations from afterward looking cameras (Aa, Ba, Ca and Da) represent energy of backscattered sunlight in

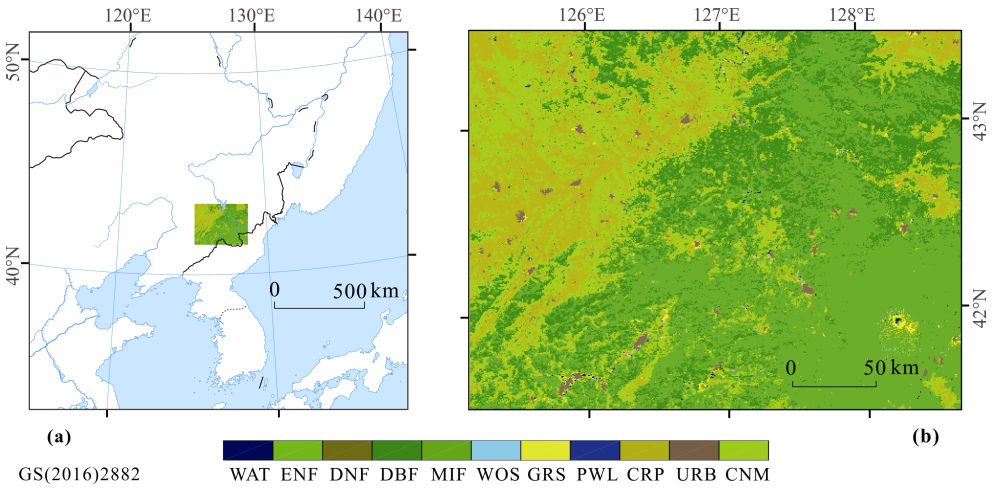

Fig. 1 Location of study area (a) and its land use and cover types (b). WAT: Water; ENF: evergreen needle leaf forest; DNF: deciduous needle leaf forest; DBF: deciduous broadleaf forest; MIF: mixed forests; WOS: woody savannas; GRS: grasslands; PWL: permanent wetlands; CRP: croplands; URB: urban and built-up; CNM: cropland/natural vegetation mosaic

Table 1 Monthly cumulative area coverage rate of MILS_BRF data in the study area during 2011–2015

Month	Jan.	Feb.	Mar.	Apr.	May	Jun.
a.c.[1] /%	18.97	21.70	32.94	98.30	93.83	80.97
data amt.[2] /%	1.64	1.51	1.42	16.96	10.38	5.20
days[3] (a.c. > 10%)	5	4	3	13	10	8
Month	Jul.	Aug.	Sep.	Oct.	Nov.	Dec.
a.c.[1] /%	75.21	69.08	95.21	99.05	96.93	23.52
data amt.[2] /%	5.65	4.69	13.89	26.40	10.42	1.83
days[3] (a.c. > 10%)	8	6	15	22	11	5

Notes: 1. Monthly cumulative area coverage (a.c.) rate. 2. The percentage of cumulative MILS_BRF data from each month relative to the total amount cover a 5-year period. 3. Days with a.c. >10%

the nominal view zenith angles of 26.1°, 45.6°, 60.0° and 70.50° respectively. Observations from the nadir camera (An) of the nominal view zenith angle of 0° represent near nadir observations. The view-sun relative azimuths are divided into three groups: principal plane (PP) ± 30° (near PP directions, nPP), cross principal plane (CP) ± 30° (near CP directions, nCP) and other (XP) azimuths. Their specific angular ranges are (0°, 30°)∪(150°, 180°), (60°, 120°), and [30°, 60°]∪[120°, 150°], respectively. Based on the 27 kinds of observation geometries, the annual overall characteristics of the observation geometry and its variation during the year were analyzed.

MODIS land cover and use products (MCD12Q1) (LP DAAC, 2017) were used to explore the spatio-temporal characteristics of MILS_BRF for different land cover types of the study area. The 'SVMScene-Classifier' parameter of MISR Level 2 TOA/Cloud Classifiers product (MIL2_SC) provides scene types of each MISR pixel (Moroney et al., 2014; MISR-Science-Team, 2015b), which is used to explore the impact of snow on MILS_BRF coverage heterogeneity in the study area.

Czapla-Myers et al. demonstrated that MISR agrees with the ground measurements to within ±1% in all four bands and has also shown long-term temporal stability (Czapla-Myers et al., 2014). Wu et al. indicated that both MODIS and MISR calibration of the reflective solar bands have been well maintained (Wu et al., 2014).

3 Results and Analysis

3.1 Intra-annual changes of MILS_BRF coverage rate

Monthly MILS_BRF coverage rate has characteristics of distinct seasonal variation. The mean of 5-yr period cumulative MILS_BRF coverage rates of 12 months in the study area is 67.14% (Table 1). The product coverage rate of the growing season is obviously higher than that of the dormant/snow cover season. During the vegetation-growth season, the product coverage rate is relatively low in July and August, marked by concentrated precipitation as compared to other months. In April and May and from September to November, product coverage rates are greater than 90%, of which the highest is in

October, at 99.05%. In December and from January to March, the product coverage rates are smaller than 33%, of which the lowest is in January, at only 18.97%. Most parts of the study area in December and from January to March have snow cover, and possibly the combination of cloud and snow cover result in product coverage rate reaching its lowest level of the year in these four months. In comparison, the product coverage rates from June to August are lower than those of other months during the growing season, which may be due to the influence of more cloudy days in these three wettest months in this region.

3.2 Spatial heterogeneity of MILS_BRF coverage

The 5-yr cumulative MILS_BRF coverage rates in most months in the study area do not show random distribution characteristics. Rather, each month has varying degrees of local aggregation (Fig. 2).

The characteristics of local aggregation of product coverage are especially clear in the four, low coverage months from December to March. During this time, agricultural areas in the central and western parts of the study area are almost data-free. In winter, these areas have a long snow cover period, thus, forming areas of singularly high reflectivity and low contrast that may result in unsuccessful MISR aerosol retrieval, and consequently the failure of MILS_BRF retrieval. In contrast, the snow cover in the eastern forest of the study area is generally below the canopy, moderating reflectivity and contrast effects. From June to August, the data poor area is mainly located in the eastern mountainous region and is attributed to the large amount of cloud cover during the precipitation-concentrated season. From April to May, there is almost no snow cover in the area, and the influence of cloud is relatively small. Thus, the coverage of BRF products is close to a random distribution. September and October also differ from the four, low-coverage months. Although there are no large areas without data, the BRF data in the centre of the study area are clearly aggregated and more abundant than that of eastern and western parts (Fig. 2). Data aggregation locations may have more clear days than other locations during September and October.

3.3 Intra-annual variation of observation geometry

Although over the whole-year, the amount of MILS_BRF data of the relative azimuth group (nPP, nCP or XP) for each off-nadir camera is similar (Table 2). This amount, as well as that of all cameras, differs significantly among months (Fig. 3, Table 3). From May to August, the amount of nCP data exceed that of nPP (Table 3). The proportion of nPP (nCP) data from each camera shows a significant difference within a single month (Fig. 3).

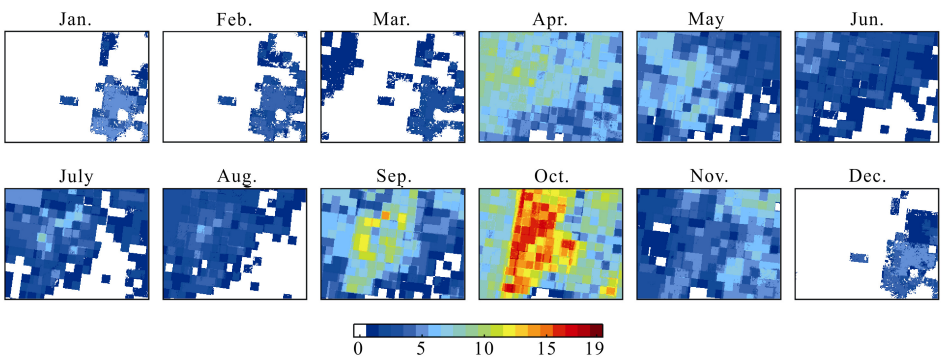

Fig. 2 The spatio-temporal changes of MILS_BRF coverage in the study area. The scale value of the colour bar represents monthly 5-yr cumulative amount of BRF data groups of each ground pixel. Each BRF data group contains data from nine observation geometries

Table 2 The proportion of MILS_BRF data from each observation geometry group to the total in the study area from 2011 to 2015 (‰)

Label	Camera									Sum
	Df	Cf	Bf	Af	An	Aa	Ba	Ca	Da	
nPP	28.74	28.37	31.41	41.56	1.33	36.03	26.18	21.00	17.85	232.47
nCP	0.52	1.22	3.16	13.09	37.32	16.19	6.42	2.40	0.68	80.98
XP	81.86	81.53	76.55	56.46	72.45	58.89	78.52	87.71	92.59	686.55

Table 3 The monthly cumulative proportion of MILS_BRF data from each group of view-sun relative azimuth (RAZ) to the total in the study area from 2011 to 2015 (‰)

RAZ	Jan.	Feb.	Mar.	Apr.	May	Jun.
nPP	5.76	3.35	1.21	11.71	4.00	1.63
nCP	0.72	0.41	0.35	6.17	8.86	8.22
XP	9.94	11.36	12.62	151.76	90.93	42.19
RAZ	Jul.	Aug.	Sep.	Oct.	Nov.	Dec.
nPP	2.01	2.94	29.46	109.14	54.84	6.42
nCP	12.71	3.52	5.17	23.21	10.34	1.31
XP	41.74	40.48	104.32	131.66	39.00	10.55

According to the data selection criterion of this study, total 22 365 171 data points of MILS_BRF observations over five years were collected. The proportions of data from each group of observation geometry to the total are shown in Table 2. The total proportion of nPP/nCP observations is 31.345%, while that of XP is 68.655%. In general, the BRDF information of land surface is concentrated in the PP directions. In order to simplify the analysis, we focused analyses on the temporal variation characteristics of the observation geometry in the nPP and nCP (perpendicular to the nPP) directions. The XP directional data are not considered separately. This section is a detailed description of these characteristics.

3.3.1 Monthly variation in amount of data between nPP and nCP

Multiple off-nadir cameras have nPP but no nCP MILS_BRF data for up to six months: four forward cameras (Df, Cf, Bf and Af) in January and February, six off-nadir cameras (Df, Cf, Bf, and Ba, Ca, Da) in September and October, seven off-nadir cameras in November (excluding Af), and all eight off-nadir cameras in December (Fig. 3). Conversely, in June and July, six off-nadir cameras (Df, Cf, Bf, and Ba, Ca Da) have nCP but no nPP data (Fig. 3).

3.3.2 Vacancy of nPP/nCP data with large view zenith

MILS_BRF data from nPP/nCP with large view zenith (Df, Cf, and Ca, Da) are not found in some months. From January to May and in August, afterward camera Ca and Da have few (Ca in January) or no nPP/nCP data. This suggests that in the two typical azimuth groups, nPP/nCP, there is nearly no BRF information for backscattered sunlight observation from zenith angle larger than 60° in the study area over the six months mentioned above. From March to May and in August, forward camera Df has no nPP/nCP data, which similarly means that with respect to nPP/nCP azimuth groups, there are also no BRF data for forward scattered sunlight observations from a nominal zenith angle of 70.50° in the study area over these four months (Fig. 3).

3.3.3 Imbalance of the amount of nPP/nCP data between forward and afterward cameras

The imbalance of the amount of MILS_BRF data within nPP/nCP between forward and afterward cameras is most prominent in January and February. In January, the amount of nPP/nCP data from afterward camera is only 8.34% of that of the forward camera, and in February only 15.22% (Fig. 3).

There are two possible causes for these three characteristics: the periodicity of the view-sun relative azimuth shift (Fig. 4) and variation in the amount of MILS_BRF data in each month across the study area (Table 1). The monthly variation in amounts of nPP and nCP observations may be primarily caused by the solar azimuth shift periodicity. Nevertheless, the characteristics of absence of nPP/nCP data with a large view zenith as well as an imbalance of the amount of data within nPP/nCP between forward and afterward cameras may be caused by the combination of these two factors. In October and November, the nadir camera has a large amount of nPP/nCP data (Fig. 3). However, our analyses shows that these data are so close to 60° and 120° relative azimuth angles, which are the boundaries between XP and nCP, that they can be practically removed from nPP/nCP groups (Fig. 4). Further discussion about the causes of these characteristics needs more relevant data support, which is beyond the scope of this paper.

3.4 MILS_BRF observation efficiency in different land cover types

The intra-annual changes of MILS_BRF observation efficiency among the four major land cover types of the study area are analyzed. The four major land cover types (and their area coverage rate) are: mixed forests (MIF, 42.41%), deciduous broadleaf forest (DBF, 17.08%), croplands (CRP, 14.52%), and cropland/natural vegetation mosaic (CNM, 24.07%). These four types cover more than 98% of the study area. The cumulative number of MILS_BRF looks per square kilometre (LPKs) from 2011 to 2015 are used to represent the MILS_BRF observation efficiency (Fig. 5).

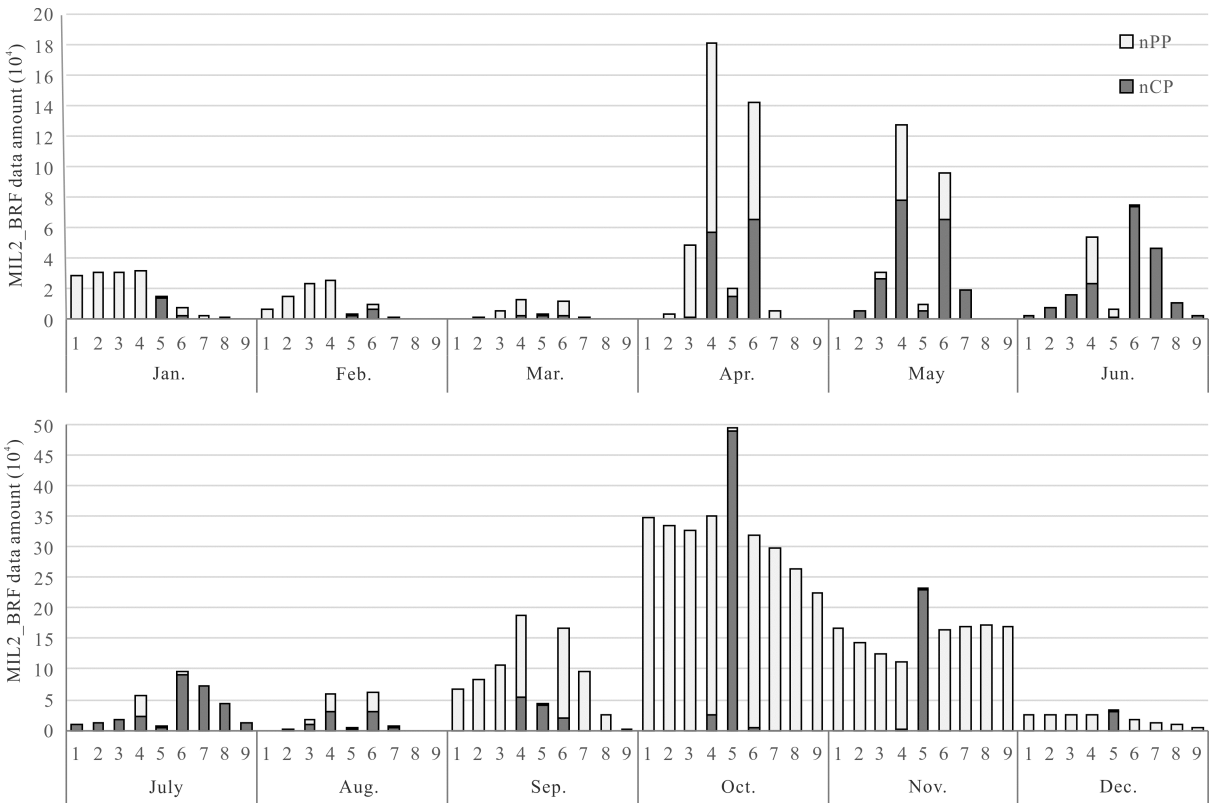

Fig. 3 Monthly cumulative amount of MILS_BRF data within nPP and nCP directions from each of the nine cameras (nine nominal view angles) during 2011–2015 period. The numbers 1–9 represent the 9 cameras (9 nominal view zenith angles) Df, Cf, Bf, Af, An, Aa, Ba, Ca, and Da of MISR, respectively

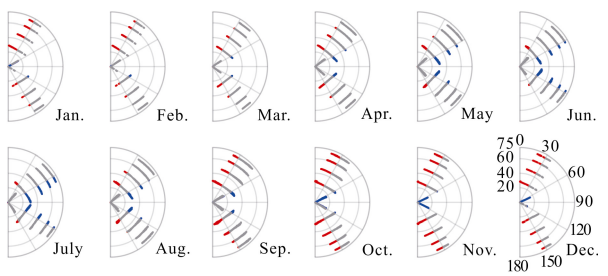

Fig. 4 Monthly variation in observation geometry of MILS_BRF data of the study area during 2011–2015. The polar angle represents the view-sun relative azimuth (0°–180°), the polar radius represents the view zenith angle (0°–75°), and the red, blue, and grey colour correspond to data within nPP, nCP, and XP, respectively

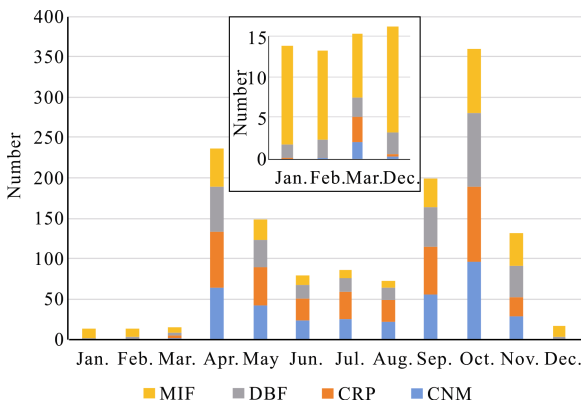

Fig. 5 The cumulative number of MILS_BRF looks per square kilometre of four major land cover types of the study area from 2011 to 2015. MIF: mixed forests; DBF: deciduous broadleaf forest; CRP: croplands, CNM: cropland/natural vegetation mosaic

During the growing season and transition months (April to November), LPKs are abundant and are almost equal among the four different land cover types. From June to August, LPKs of MIF and DBF are less than those of CRP and CNM. This appears to be the result of greater rainy-season cloudiness in the MIF and DBF areas, located in the southeast mountainous part of the study area, than the CRP and CNM areas.

In contrast, the vegetation dormancy season (from December to March) observes a small number and very uneven proportions of LPKs (Fig. 5 inset), from which there were no MILS_BRF data for CRP and CNM from December to February, and a small amount for DBF. In these three months, most of LPKs are concentrated on

MIF while MILS_BRF data begin to appear in CRP and CNM in March.

Therefore, the observation geometry variation of MILS_BRF from December to February largely reflects the observation characteristics for MIF and DBF (section 3.3). In contrast, from March to November, it is the common characteristics for the four main land cover types (section 3.3). The four months from December to March are the core snow-covered period in the study area, and the relationship between the spatio-temporal characteristics of MILS_BRF and snow presence will be discussed in section 4.1.

4 Discussion

4.1 Semi-permanent data-poor areas of MILS_BRF

Our study suggests that snow cover causes the semi-permanent data-poor area of MILS_BRF from December to February. This is based on MIL2_SC data from 2011 to 2015, 5-yr of MISR 'Snow_Ice' observations for each pixel in December, January and February (Fig. 6). Subregions with a high frequency of 'Snow_Ice' are also located in the central and western parts of the study area, corresponding with the MILS_BRF data gaps (Fig. 2). This 5-year period result enhances the finding that the snow-ice surface was almost data-free in the 2006 global MISR Albedo product (Liao et al., 2014).

The semi-permanent data-free areas of MILS_BRF in the study area are mainly composed of pixels with an MIL2_SC value of 'Snow_Ice'. This finding provides a potential direction to fill the data-free area. In fact, 'Snow_Ice' pixels are also clear sky pixels (Moroney et al., 2014). Although snow covered surface with high reflectance and low contrast often results in the failure of aerosol retrieval (Abdou et al., 2006), MISR cameras receive radiance energy from these pixels without the impediment of clouds. Therefore, with consideration of the characteristic of snow cover surface, it may be possible to fill these data-free areas by developing a specific aerosol retrieval method that is different from the existing algorithm. Alternatively, He et al., (2017) attempted to directly estimate land surface albedo using the clear sky MISR top of atmosphere BRF rather than relying on aerosol retrievals. From this perspective, it may be possible to directly retrieve land surface BRF of clear sky snow-covered area.

4.2 Significance of spatio-temporal characteristics of MILS_BRF coverage

Spatio-temporal characteristics of MILS_BRF product coverage are significant in evaluating the reliability of albedo products. One needs to consider the spatio-temporal characteristics of MILS_BRF coverage rate/location over a given area to avoid any misleading interpretations due to difference in data availability across seasons or land-cover types. Pinty et al. (2011) and Liao et al. (2014) considered the impact of MISR product coverage on albedo products derived from observation of MISR and other sensors. Liao et al. (2014) did not explicitly analyze nor give the spatio-temporal characteristics of MISR products but acknowledged that the results were not a true 'global average' but an average of all available data. Pinty et al. (2011) pointed out that the robustness of accompanying statistics declines with the reduction of the number of MISR observation samples.

Pinty et al. (2011) and results of this paper are compared in Fig. 7. The blue line is the average MISR sampling efficiency profile of 2006 at the latitude of 42.5°N extracted from Fig. 1 in Pinty et al., (2011). The red line is the percentage of cumulative data amount of MILS_BRF from 2011 to 2015 in the study area of this paper. At 42.5°N, snowing occurs in most areas of the land of the Earth from December to March, corresponding with the four months of lowest sampling efficiency in the whole year. Our study area shared this characteristic. However, during June, July and August, there exist great differences in cloud cover in different climatic zones at 42.5°N. In our study area, rainy clouds frequently appear during this time, which may be the reason why sample values are significantly lower than the average at the same latitude.

As a summary, due to the difference between the underlying surface and the local climate, and in order to

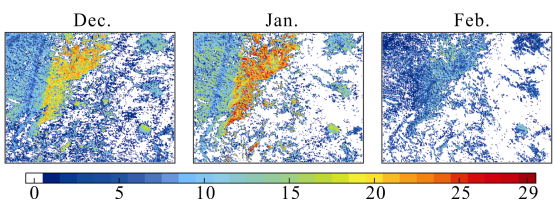

Fig. 6 5-yr cumulative MISR 'Snow_Ice' observations in December, January and February during 2011–2015

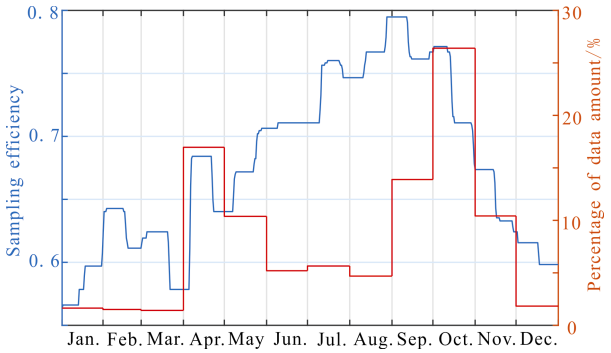

Fig. 7 Comparison of monthly data amount percentage of MILS_BRF in the study area of this paper (red line) and the average sampling efficiency of MISR on the same latitude of 42.5°N (blue line)

ensure reliability of the comparison results, it is necessary to analyze the spatio-temporal variation of product coverage in one's specific research area, rather than simply relying on the latitude (or longitude) average when comparing MISR and other satellite albedo products.

4.3 Impact of monthly variation of observation geometry on BRDF model evaluation

The principal plane and its vicinity are generally the focus of accuracy evaluation of the BRDF model, accounting for the cross principal plane and its vicinity (Hu et al., 1997; Lucht, 1998; Huang et al., 2013). Our analyses (section 3.3) indicate that when using MILS_BRF data to analyze the performance and accuracy of BRDF model from the perspective of azimuth of nPP (nCP) directions and different view zenith angles, one has to consider intra-annual variation of observation geometry of MILS_BRF data. Otherwise, the results of the analysis may be due to the response of the BRDF model to seasonal variation of the observation geometry of MILS_BRF, rather than the characteristics of the BRDF model itself. This is consistent with the observation that reflectance products of MISR are not sufficient to analyze the extrapolation ability of the BRDF model parameters products at all viewing angles (Chen et al., 2009).

Our analyses is not limited to discrete sites and times but an extensive area and five years of data, allowing examination of a range of MISR observation geometry variation (Figs. 3 and 4). For example, from May to July, MILS_BRF in the study area has almost no nPP data (red points on Fig. 4) at large zenith angle. In comparison, from September to November nPP data are abundant at each zenith angle. Therefore, if the accuracy of a BRDF model is evaluated by MILS_BRF alone, even if MILS_BRF for an entire year is used, results for the nPP performance of the BRDF model will only represent the characteristics of the land surface from September to November. Armston et al. (2007) presented similar concerns that further analysis of the sensitivity of the BRDF model inversion to acquisition geometry is required, which will help determine the environmental noise equivalence of the MISR surface BRF's and BRDF model parameters.

5 Conclusions

In this study, the spatio-temporal distribution of coverage and observation geometry of the MISR land-surface BRF product (MILS_BRF) were analyzed and explored over a typical study area in central Northeast Asia from 2011 to 2015. The results further our knowledge of the spatio-temporal characteristics and observation limitations of MILS_BRF in the study area.

The results and analysis of this paper demonstrate that when using MILS_BRF to assess the accuracy of BRDF model, it is necessary to consider its spatio-temporal characteristics of product coverage and observation geometry. First, the intra-annual variation of coverage rate/location of MILS_BRF observations need to be considered to avoid misleading interpretation due to the difference of data availability in different months or land-surface types. Further, when analysing the accuracy of BRDF model in terms of nPP/nCP directions or view zeniths, one has to consider the characteristics of monthly variation of MILS_BRF observation geometry to carefully discern the performance of BRDF model itself from the intra-annual variation pattern of MILS_BRF observation geometry.

From the perspective of the final product beyond on-satellite observations, the findings of this study reveal a new perspective on product spatial coverage and observation geometry for multi-angle remote sensing. In particular, the identification of a large data-free area that is mainly composed of crop lands and a mosaic of cropland/natural vegetation in the study area for four consecutive winter months provides a potential direction for improving the MILS_BRF retrieval algorithm. The analysis in this study also can be extended to other lar-

ger or even global scales, to provide a complete reference to strengths and limitations of MILS_BRF for users.

References

Abdou W A, Pilorz S H, Helmlinger M C et al., 2006. Sua Pan surface bidirectional reflectance: a case study to evaluate the effect of atmospheric correction on the surface products of the Multi-angle Imaging SpectroRadiometer (MISR) during SAFARI 2000. *IEEE Transactions on Geoscience and Remote Sensing*, 44(7): 1699–1706. doi: 10.1109/TGRS.2006.876031

Angal A, Xiong X X, Wu A S, 2017. Monitoring the on-orbit calibration of terra MODIS reflective solar bands using simultaneous terra MISR observations. *IEEE Transactions on Geoscience and Remote Sensing*, 55(3): 1648–1659. doi: 10.1109/TGRS.2016.2628704

Armston J D, Scarth P F, Phinn S R et al., 2007. Analysis of multi-date MISR measurements for forest and woodland communities, Queensland, Australia. *Remote Sensing of Environment*, 107(1–2): 287–298. doi: 10.1016/j.rse.2006.11.003

Bruegge C J, Val S, Diner D J et al., 2014. Radiometric stability of the multi-angle imaging spectroradiometer (MISR) following 15 years on-orbit. In: *Proceedings of the SPIE 9218*, *Earth Observing Systems XIX*. San Diego, California, USA: SPIE, 9218: 92180N. doi: 10.1117/12.2062319

Bull M, Matthews J, McDonald D et al., 2011. *MISR Data Product Specifications Document* (*JPL D-13963*, *Revision S*). Pasadena: Jet Propulsion Laboratory, California Institute of Technology.

Chen Yongmei, Wang Jindi, Liang Shunlin et al., 2009. Comparison of MISR and MODIS bidirectional reflectance products. *Journal of Remote Sensing*, 13(5): 808–820. (in Chinese)

Chen Y M, Wang J D, Liang S L et al., 2008. The bidirectional reflectance signature of typical land surfaces and comparison of MISR and MODIS BRDF products. In: *Proceedings of 2008 IEEE International Geoscience and Remote Sensing Symposium*. Boston, MA, USA: IEEE, III-1099–III-1102. doi: 10.1109/IGARSS.2008.4779546

Czapla-Myers J, Thome K, Anderson N et al., 2014. The absolute radiometric calibration of Terra imaging sensors: MODIS, MISR, and ASTER. In: *Proceedings of the SPIE 9218*, *Earth Observing Systems XIX*. San Diego, California, USA, 9218: 92180Y. doi: 10.1117/12.2062529

Diner D J, Martonchik J V, Borel C et al., 2008. *Multi-angle Imaging SpectroRadiometer (MISR) Level 2 Surface Retrieval Algorithm Theoretical Basis* (*JPL D-11401*, *Revision E*). Pasadena: Jet Propulsion Laboratory, California Institute of Technology.

He T, Liang S L, Wang D D, 2017. Direct estimation of land surface albedo from simultaneous MISR data. *IEEE Transactions on Geoscience and Remote Sensing*, 55(5): 2605–2617. doi: 10.1109/TGRS.2017.2648847

Hu B X, Lucht W, Li X W et al., 1997. Validation of kernel-driven semiempirical models for the surface bidirectional reflectance distribution function of land surfaces. *Remote Sensing of Environment*, 62(3): 201–214. doi: 10.1016/S0034-4257(97)00082-5

Huang X Y, Jiao Z T, Dong Y D et al., 2013. Analysis of BRDF and albedo retrieved by kernel-driven models using field measurements. *IEEE Journal of Selected Topics in Applied Earth Observations and Remote Sensing*, 6(1): 149–161. doi: 10.1109/JSTARS.2012.2208264

Liao Yao, Lü Daren, He Qing, 2014. Intercomparison of albedo product retrieved from MODIS, MISR and POLDER. *Remote Sensing Technology and Application*, 29(6): 1008–1019. (in Chinese)

Liu X, Kafatos M, 2007. MISR multi-angular spectral remote sensing for temperate forest mapping at 1.1-km resolution. *International Journal of Remote Sensing*, 28(2): 459–464. doi: 10.1080/01431160601075491

LP DAAC, 2017. Land cover type yearly L3 global 500 m SIN Grid. https://lpdaac.usgs.gov/dataset_discovery/modis/modis_products_table/mcd12q1

Lucht W, 1998. Expected retrieval accuracies of bidirectional reflectance and albedo from EOS-MODIS and MISR angular sampling. *Journal of Geophysical Research*: *Atmospheres*, 103(D8): 8763–8778. doi: 10.1029/98JD00089

Lucht W, Lewis P, 2000. Theoretical noise sensitivity of BRDF and albedo retrieval from the EOS-MODIS and MISR sensors with respect to angular sampling. *International Journal of Remote Sensing*, 21(1): 81–98. doi: 10.1080/ 014311600211000

Mahtab A, Sridhar V N, Navalgund R R, 2008. Impact of surface anisotropy on classification accuracy of selected vegetation classes: an evaluation using multidate multiangular MISR data over parts of Madhya Pradesh, India. *IEEE Transactions on Geoscience and Remote Sensing*, 46(1): 250–258. doi: 10.1109/TGRS.2007.906157

MISR-Science-Team, 2015a. Terra/MISR Level 2 land surface data, version 2 retrieved from March 31, 2016 to March 30, 2017, from NASA ASDC. doi: 10.5067/Terra/MISR/MIL2ASLS_L2.002

MISR-Science-Team, 2015b. Terra/MISR level 2 TOA/Cloud classifiers, version 3 retrieved from Dec 31, 2017 to Feb 28, 2018, from NASA Atmospheric Science Data Center (ASDC). doi: 10.5067/Terra/MISR/MIL2TCCL_L2.003

Moroney C, DiGirolamo L, Jones A, 2014. *MISR Data Products Specifications for the MISR Level 2 Classifiers Product* (*JPL D-81127*, *Revision A*). Pasadena: Jet Propulsion Laboratory, California Institute of Technology.

Nag S, Gatebe C K, de Weck O, 2015. Observing system simulations for small satellite formations estimating bidirectional reflectance. *International Journal of Applied Earth Observation and Geoinformation*, 43: 102–118. doi: 10.1016/j.jag.2015. 04.022

Nag S, Gatebe C K, Hilker T, 2017. Simulation of multiangular remote sensing products using small satellite formations. *IEEE Journal of Selected Topics in Applied Earth Observations and Remote Sensing*, 10(2): 638–653. doi: 10.1109/Jstars.2016.2570683

Pinty B, Taberner M, Haemmerle V R et al., 2011. Global-scale comparison of MISR and MODIS land surface albedos. *Journal of Climate*, 24(3): 732–749. doi: 10.1175/2010JCLI3709.1

Taberner M, Pinty B, Govaerts Y et al., 2010. Comparison of MISR and MODIS land surface albedos: methodology. *Journal of Geophysical Research*: *Atmospheres*, 115(D5): D05101. doi: 10.1029/2009jd012665

Wanner W, Strahler A H, Hu B et al., 1997. Global retrieval of bidirectional reflectance and albedo over land from EOS MODIS and MISR data: theory and algorithm. *Journal of Geophysical Research*: *Atmospheres*, 102(D14): 17143–17161. doi: 10.1029/96jd03295

Wu A S, Angal A, Xiong X X, 2014. Comparison of coincident MODIS and MISR reflectances over the 15-year period of EOS terra. In: *Proceedings of the SPIE 9218*, *Earth Observing Systems XIX*. San Diego, California, USA: SPIE, 9218: 92180W. doi: 10.1117/12.2061117

Wu H Y, Liang S L, Tong L et al., 2011. Snow BRDF characteristics from MODIS and MISR data. In: *Proceedings of 2011 IEEE International Geoscience and Remote Sensing Symposium*. Vancouver, BC, Canada: IEEE, 3187–3190. doi: 10.1109/IGARSS.2011.6049896